Simulation of Transient Photoconduction in Organic p−n Junction Bilayer Photodiodes

Li Tan,[†] M. David Curtis,[†,‡] and A. H. Francis*[,‡]

Macromolecular Science & Engineering Center, and Department of Chemistry, The University of Michigan, Ann Arbor, Michigan 48109-1055

Received October 31, 2003. Revised Manuscript Received March 30, 2004

The transient photoconducting behavior of organic p/n bilayer photocells has been investigated in cells constructed with the copolymer, poly(3-butylthiophene-*co*-ethylenedioxythiophene), as p-type material and a perylene diimide (PV) as the n-type material. The decay rate constant of the transient photocurrent observed after pulsed illumination is independent of the applied electric field, light intensity, and temperature. However, the peak photoresponse was strongly affected by these variables. Simulations of the photoresponse revealed that the peak current depends primarily on the carrier mobility (at a given light intensity), whereas the characteristic decay rate is hardly influenced by the mobility, but depends on the carrier lifetime which is chiefly due to trapping by deep levels.

Introduction

Photoconduction involves three fundamental steps: (1) absorption of photons by the material with the subsequent production of coulomb-bound, electron−hole (e−h) pairs; (2) separation of e−h pairs into free carriers; and (3) charge transport by the free carriers.[1] In organic photoconductors, excitons generated in the first step are essentially localized on single molecules and have e−h binding energies on the order of 0.5−1 eV. The binding energies are sufficiently large that the efficiency of charge separation when bulk organic material is photoexcited into its first excited singlet is relatively low. As a result, charge separation is believed to occur primarily at interfaces and defect sites[1−4] where it is facilitated by the energy available when an electron is transferred from a higher to a lower energy level, for example, from a donor to an acceptor. The interface may be between two organic materials (a "p/n" junction) or between an electrode and the photoactive material. (The "p/n" terminology employed here follows current convention; however, the hole- and electron-transporting layers are not p- or n-doped, respectively. Rather, the terminology refers to the character of the photoexcited majority carriers in each material.)

We have demonstrated previously that the action spectrum of the bilayer photodiode (ITO/polymer/PV/Au) followed the absorption spectrum of the PV (1,2-diaminobenzene perylene-3,4,9,10-tetracarboxylic acid diimide) under illumination from the ITO side, but followed the spectrum of the polymer under illumination from the Au side.[5] These observations were interpreted to mean that charge generation and separation occurred when light was absorbed at the polymer/PV interfacial layer and that both the polymer and PV were actively involved in the photogeneration of carriers. Thus, only when excitons are produced at, or diffuse to, the p/n junction or to an electrode interface can they dissociate efficiently to generate free carriers.[1−4] The photoresponse occurs as these carriers are generated and transported through the bulk layer.

In this paper, we report our investigations of the transient photoresponse of layered, p/n junction photocells in which the copolymer, poly(3-butylthiophene-*co*-ethylenedioxythiophene) (P3BT-*co*-EDOT), was used as the hole-transporting ("p-type") layer and PV as the electron-transporting ("n-type") layer.[5−7] This approach has been a valuable tool to probe photoconduction in single-layer organic devices based on tetracene, pentacene, and polydiacetylene crystals.[8−10] Previous investigations of single-layer photocells have ignored the influence of interface-assisted exciton dissociation as excitons were produced only in the bulk of a homogeneous single layer.[2a,10] The transient photocurrent can be analyzed to provide valuable data on intrinsic properties, for example, carrier lifetime and mobility. Simulations are reported here in which sheets of charge

* To whom correspondence should be addressed.
[†] Macromolecular Science & Engineering Center.
[‡] Department of Chemistry.

(1) Review articles: (a) Gregg, B. A. *J. Phys. Chem. B* **2003**, *107*, 4688. (b) Gregg, B, A.; Hanna, M. C. *J. Appl. Phys.* **2003**, *93*, 3605. (c) Peumans, P.; Yakimov, A.; Forrest, S. R. *J. Appl. Phys.* **2003**, *93*, 3693.
(2) (a) Binh, N. T.; Gailberger, M.; Bässler, H. *Synth. Met.* **1992**, *47*, 77−86. (b) Bonham, J. S. *Aust. J. Chem.* **1976**, *29*, 2123. (c) Pope, M.; Swenberg, C. E.; *Electronic Processes in Organic Crystals and Polymers*, 2nd ed.; Oxford Scientific Publications: Oxford, 1999.
(3) (a) Danziger, J.; Dodelet, J.-P.; Lee, P.; Nebesny, K. W.; Armstrong, N. R. *Chem. Mater.* **1991**, *3*, 821. (b) de Bettignies, R.; Nicolas, Y.; Blanchard, P.; Levillain, E.; Nunzi, J.-M.; Roncali, J. *Adv. Mater.* **2003**, *15*, 1939. (c) Halls, J. J. M.; Cornil, J.; dos Santos, D. A.; Silbey, R.; Hwang, D.-H.; Holmes, A. B.; Brédas, J. L.; Friend, R. H. *Phys. Rev. B* **1999**, *60*, 5721.
(4) (a) Tang, C. W. *Appl. Phys. Lett.* **1986**, *48*, 183. (b) Gregg, B. A.; Fox, M. A.; Bard, A. J. *J. Phys. Chem.* **1990**, *94*, 1586.
(5) Tan, L.; Curtis, M. D.; Francis, A. H. *Chem. Mater.* **2003**, *15*, 2272.
(6) Maki, T.; Hashimoto, H. *Bull. Chem. Soc. Jpn.* **1952**, *25*, 411.
(7) Hiramoto, M.; Fukusumi, H.; Yokoyama, M. *Appl. Phys. Lett.* **1992**, *61*, 2580.
(8) Reimer, B.; Bässler, H. *Phys. Status Solidi B* **1978**, *85*, 145.
(9) Moses, D.; Sinclair, M.; Heeger, A. J. *Phys. Rev. Lett.* **1987**, *58*.
(10) Silinsh, E. A.; Kolesnikov, V. A.; Muzikante, I. J.; Balode, D. R. *Phys. Status Solidi B* **1982**, *113*, 379.

10.1021/cm035102d CCC: $27.50
Published on Web 05/04/2004

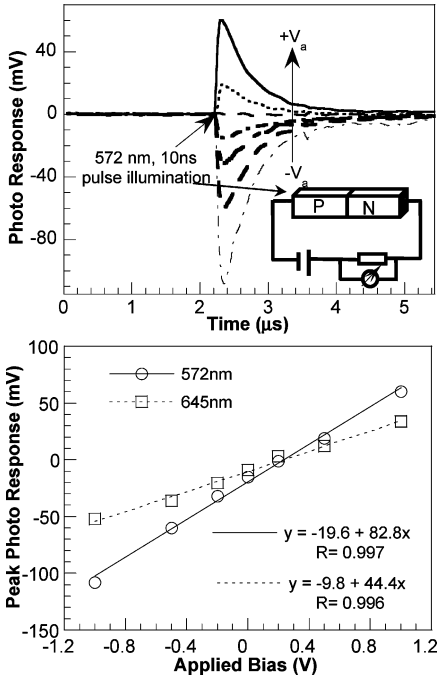

Figure 1. Transient response of ITO/P3BT-*co*-EDOT/PV/Ag with 10-ns pulse. (top) Response at various applied fields (λ = 572 nm, voltage ranges from −1 to +1 V); (bottom) linear relationship between peak photoresponse and applied bias at different excitation wavelengths (λ = 572 or 645 nm).

carriers generated at the organic p/n interface are transported toward the electrodes. Signal decay is caused by a short carrier lifetime rather than by carrier extraction at the electrodes, and the peak photocurrent is primarily a function of the carrier mobility as well as the number of carriers generated at the p/n interface.

Experimental Section

The transient photoresponse was stimulated by a 10-ns nitrogen laser pulse (λ = 337 nm). Studies of the wavelength dependence of the photoresponse employed the nitrogen laser to pump a dye laser providing 10-ns duration pulsed excitation in the visible, between 450 and 680 nm. The laser intensity was attenuated by insertion of neutral density filters to examine the dependence of a transient signal on laser power. The temperature dependence of the photoresponse was studied by placing the photocell in a cryostat and cooling in a temperature-regulated flow of nitrogen gas. The experimental circuit is shown in Figure 1 (inset), which depicts the p/n bilayer photocell in series with a voltage source and a load resistor. The photocell is shown in the reverse biased configuration (−V); however, measurements were also conducted in the forward (+V) biased configuration. In each case, the photoinduced transient signal was measured in the "current" or "short circuit" mode in which the RC time constant of the measuring instrument is much less than the response time of the photocell. The response time of the measuring circuitry was approximately 50 ns and was determined principally by distributed capacitance and the capacitance of the photocell. The signal was measured as a voltage drop across the load resistor (50−330 Ω). In the reverse bias configuration shown, transient photocurrent flows counterclockwise, defined as negative current flow, and is detected as a negative voltage across the load resistor. In the forward bias configuration, transient photocurrent flows clockwise (positive current) and is detected as a positive voltage transient across the load resistor. The transient voltage signal was captured by a PAR Model 164, "boxcar" integrator, and stored digitally.

To directly compare the experimental photoresponse with that obtained from simulations, it was necessary to include the finite bandwidth of the instrumentation in the simulation. This was accomplished by convolution of the simulated response function $V(t)$ with the instrument response function $H(t)$ to obtain $F(t)$, the simulated response as modified by the instrument response. Thus,

$$F(t) = \int_0^\infty H(\tau)V(t - \tau)\, d\tau$$

The convolution was carried out for a discrete number of data points M sufficient to define the envelope of the photoresponse,

$$F(i) = \sum_{j=1}^{M} H(j)V(i - j)$$

$H(t)$ could be determined directly by measuring the impulse response of the instrument with the same circuit impedance used for the experimental measurements. $H(t)$ was found to be determined chiefly by the bandwidth of the boxcar integrator.

Results

The transient photoresponses of the p/n photocell, ITO/P3BT-*co*-EDOT (1200 Å)/PV (800 Å)/Ag, were measured. Examples of the transient responses are shown in Figure 1. The typical phototransient signal consisted of a fast response (∼0.1 μs duration) coincident with the laser excitation pulse, followed by a slower decay with an exponential dependence ($\tau \sim 0.5$ μs at ambient temperture).

Electric Field Dependence. The effect of bias voltage on the photoresponse of the p/n photocells is shown in Figure 1. In the reverse biased configuration, the peak photoresponse became more negative with increasing reverse bias. Without bias a negative photoresponse was always obtained due to the photovoltaic effect.[11] As shown in Figure 1 (top), the photoresponse became increasingly positive when a forward bias was applied. A positive photocurrent was observed when the forward bias exceeded the open circuit voltage (V_{oc}), which is determined by the light intensity and the difference in the work functions of the two electrodes.[2b,12] A plot of peak photoresponse (voltage) vs the applied bias gave the linear relationship shown in Figure 1 (bottom). The photoresponse exhibited an exponential decay with a 0.5−0.6-μs characteristic decay time that was essentially independent of the applied electric field strength, as illustrated by the comparison of the normalized photoresponse curves obtained at different bias conditions shown in Figure 2.

Illumination Dependence. Illumination of the ITO/polymer/PV/Ag bilayer photocells with various dye laser wavelengths (337, 480, 572, 605, or 645 nm) produced a similar transient photoresponse (Figure 1S, bottom (Supporting Information)). The temperature dependence of the peak photoresponse was also independent of excitation wavelength (in the range investigated), suggesting that the initially prepared photoexcited state relaxes rapidly and that thermal equilibrium is established before the exciton dissociation event occurs. A short positive transient is produced by illumination at

(11) It is possible to reverse the sign of the short circuit photocurrent under conditions that lead to electron injection from the back electrode. See refs 2b, 5, and 12.

(12) (a) Stimming, U. *Langmuir* **1987**, *3*, 423. (b) Malliaris, G. G.; Salem, J. R.; Brock, P. J.; Scott, J. C. *J. Appl. Phys.* **1998**, *84*, 1583.

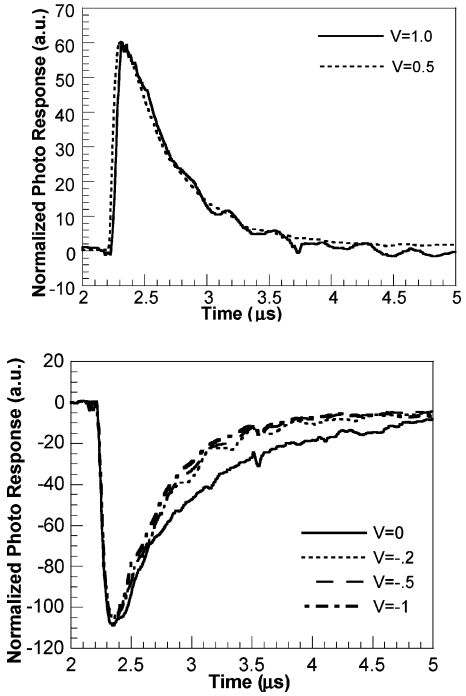

Figure 2. Normalized transient photoresponses of ITO/P3BT-*co*-EDOT/PV/Ag: (top) $V_a = 0.5$, 1.0 V; (bottom) $V_a = 0.0$, −0.2, −0.5, −1.0 V, $\lambda_{exc} = 572$ nm.

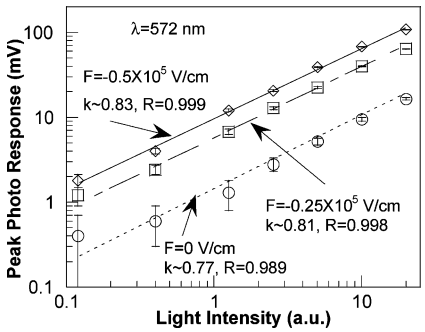

Figure 3. Dependence of peak transient photoresponse (ITO/P3BT-*co*-EDOT/PV/Ag) on the intensity of the illumination ($\lambda = 572$ nm) under different applied biases: $F_a = 0.0$, -2.5×10^4, and -5×10^4 V/cm.

337 nm (see Figure 2S-a (Supporting Information)) because significant intensity is transmitted by the p/n layers at 337 nm and stimulates photoemission from the back electrode. This conclusion is supported by the observation that the transient was suppressed when a metal with higher work function (Au) was used as the back electrode. The positive transient was also suppressed when the cell was illuminated with light of a wavelength that was strongly absorbed by the polymer or PV ($\lambda = 480$, 572, or 645 nm, Figure 1S) or when the Ag electrode was biased positively ($\lambda = 337$ nm in Figure 2S-b). A log−log plot (Figure 3 and Figure 3S (Supporting Information)) of the peak photocurrent response (j_p) versus illumination intensity (I) reveals a power law relationship between these quantities, $|j_p| = aI^k$. The slope (k) of the linear fitting is slightly field-dependent, increasing from +0.77 at zero field to +0.83 at -5×10^4 V/cm.

Temperature Dependence. The temperature dependence of the transient photoresponse was measured over a limited temperature range and is shown in Figure 4 (top). The peak photoresponse decreased as the temperature was lowered. Plots of $\log(|j_p|)$ vs $1/T$ for different field values (see Figure 4S Supporting Information) were approximately linear ($R \geq 0.95$) and yielded activation energies for charge carrier photoproduction (inferred from the slopes) that decreased from a value of 128 meV at zero field to 45 meV at 10^5 V/cm. The characteristic relaxation time was independent of temperature as shown in Figure 5S (Supporting Information).

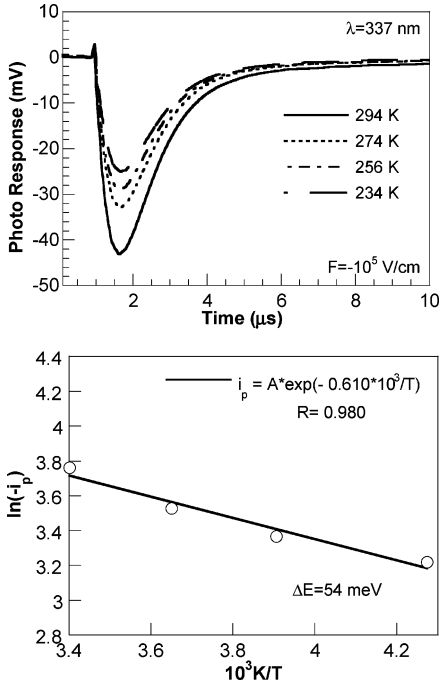

Figure 4. Transient photoresponses of ITO/P3BT-*co*-EDOT/PV/Ag at different temperatures with illumination from ITO side (top); $\log(j_p)$ vs $1/T$ (bottom).

Discussion

The photogeneration process in the bilayer devices described here occurs primarily at the organic p/n junction, as has been demonstrated by previous studies of photocurrent action spectra of these bilayer devices.[3−5] Charge-neutral singlet (S_1) Frenkel excitons (e−h pairs) are efficiently produced by photoexcitation throughout both p- or n-type organic layers. Steady-state concentrations of S_1 excitons and free charge carriers are established during the light pulse on the nanosecond time scale. However, the rate of generation of free charge carriers by dissociation of S_1 excitons is determined by photoexcitation within exciton migration distances of the p/n or electrode/organic interfaces. When P3BT/EDOT excitons are proximate to the p/n interface, charge separation may occur by the transfer of an electron from the P3BT/EDOT LUMO to the lower energy LUMO of PV if the energy gained by electron transfer exceeds the binding energy of the e−h pair. Similarly, PV excitons in the region of the p/n interface may dissociate by transfer of the hole from the PV HOMO to the HOMO of P3BT. Again, the energy gained by the hole relaxation must be greater than the binding energy of the exciton. Thus, excitation of either side of the p/n junction produces charge separation with P3BT positive (excess holes) and PV negative (excess electrons). The built-in field[2b,12b] of the cell is such that holes

drift toward ITO and electrons toward the Ag electrode. The drift is aided by a reverse bias and opposed by a forward bias.

Qualitatively, the current−time behavior of the cell can be understood as follows: Let a thin sheet of negative charge, generated at $t = 0$ at the p/n interface, be transported with constant velocity toward the back electrode by an applied or built-in electric field. If there is no decay in the number of carriers during the transport, the current will be constant until the sheet of charge encounters the back electrode where the carriers are discharged and the current suddenly drops to zero. The total charge in the sheet of carriers is given by $Q = N_0 e = \int i \, dt = i_p \tau_{tr}$, where N_0 is the initial concentration of electrons generated by the light pulse, e the electronic charge, i_p the peak current, and τ_{tr} the transit time, equal to the time at which the current drops to zero. The transit time is related to the electron mobility by $\mu_n = L_2^2/V_2\tau_{tr}$, where μ_n is the electron mobility, L_2 is the thickness of the n-type material, and V_2 is the voltage drop across L_2. Hence, $i_p = N_0 e V \mu_n / L_2^2 = N_0 e F \mu_n / L_2$. Thus, for a field-independent mobility, the peak current is directly proportional to the applied field, the initial concentration of carriers, and the carrier mobility. Diffusion of the carrier sheet during its transit does not affect the magnitude of the current because as many carriers are diffusing "backward" as there are diffusing "forward". However, the spatial distribution of charges is important in determining the shape of the $i(t)$ curve near $t = \tau_{tr}$ as the leading edge of the carrier packet reaches the electrode and charge extraction dominates the current characteristics.

If the carriers have a finite lifetime, τ, then $N(t) = N_0 \exp[-t/\tau]$, and the current decays exponentially with time from its peak value, $i_p(0)$. If the lifetime is sufficiently short, the current can completely decay before the carriers encounter the electrode, and no "kink" will appear in the $i(t)$ vs t curve to mark the transit time. This situation obtains for the devices described in this paper.

Similar considerations apply to the sheet of positive carriers transversing the p-type polymer layer to the front electrode. The total current is the sum of the electron and hole currents, $i = (N_0 eF/L)(\mu_+ \exp[-t/\tau_+] + \mu_- \exp[-t/\tau_-])$, setting $L_1 + L_2 = L$. If one of the mobilities is larger than the other by a factor of 10 or more, the motion of that carrier dominates the peak current. Likewise, the longer-lived carrier dominates the current−time curve at longer times, and the initial, rapid decay of the shorter-lived carrier may be masked by the RC delay in the cell and measuring circuitry.

Quantitatively, the displacement of carriers induces a space average current $j(t)$ in the external circuit given by[13]

$$j(t) = \frac{1}{L}\left\{\int_0^L [j_p(x,t) + j_n(x,t)]\, dx + \epsilon \frac{dF(x,t)}{dt}\right\} \quad (1)$$

In eq 1, a one-dimensional approximation is used for the motion of the charge carriers, with the direction of motion confined to the x-axis. In the experiments, a constant electric field F is maintained ($dF/dt = 0$) during the transient measurement, and changes in the field across the sample induced by the moving carriers generate a current, $j(t)$. The observed transient photoresponse represents the kinetics of charge generation, transport, and relaxation in the P3AT and PV material layers.

The transport equations for the excess photogenerated charge carriers (hole or electron, p or n) after the light pulse are given by eqs 2−3 (note: the following treatment ignores any charge generation at the electrode interfaces as well as bimolecular e−h recombination):

$$\frac{dp}{dt} = -\frac{p}{\tau_p} - \frac{1}{q}\frac{dj_p}{dx} \quad (2)$$

$$\frac{dn}{dt} = -\frac{n}{\tau_n} + \frac{1}{q}\frac{dj_n}{dx} \quad (3)$$

These equations apply to the majority carriers (holes in polymer and electrons in PV) generated in these materials by photons absorbed near the p/n junction. The equations can be rewritten with the aid of the following expressions for the current density:

$$j_p = qp\mu_p F + qD_p \frac{dp}{dx} \quad (4)$$

$$j_n = qn\mu_n F + qD_n \frac{dn}{dx} \quad (5)$$

D is the diffusion coefficient for the carriers and is assumed in the following to obey the Einstein relationship, $D = \mu kT/q$. Substituting eq 4 into eq 2 and setting $dF/dx = 0$ yields eq 6.

$$D_p \frac{d^2p}{dx^2} - \mu_p F \frac{dp}{dx} = \frac{dp}{dt} + \frac{p}{\tau_p} \quad (6)$$

The equation obtained for electrons is identical except for the sign of the term containing the mobility. Solutions of eq 6 depend on the choice of boundary conditions. If it is assumed that carrier extraction at the electrodes maintains zero carrier concentration at the electrodes, then the boundary conditions are

$$p(x = 0, t = 0+) = p(x = L, t = 0+) = 0$$

and solutions are obtained as

$$p(x,t) = \sum_{n=1}^{\infty} A_n \sin\left(\frac{n\pi x}{L}\right) \exp\left[-\left(\frac{1}{\tau_p} + D_p\left(\frac{n\pi}{L}\right)^2\right)t\right] \quad (7)$$

where L is the overall thickness of the bilayer photocell and the coefficients are given by

$$A_n = \frac{2}{L}\int_0^L p(x,0) \sin\left(\frac{n\pi x}{L}\right) dx$$

Evaluation of the coefficients requires knowledge of $p(x,0)$, the initial spatial distribution of photogenerated holes. The carriers (holes in the polymer and electrons in the PV) produced during the 10-ns laser flash are initially confined to a thin sheet at the p/n interfacial layer. For the purpose of the calculation, the interface is chosen to lie in the middle of the device at $x = L/2$ and the initial hole distribution was represented by a

(13) Scher, H.; Shlesinger, M. F.; Bendler, J. T. *Phys. Today* **1991**, Jan, 26−34.

δ-function at $x = L/2$. The coordinate system of the calculation is shown in Figure 6S (Supporting Information). Thus,

$$p(x,t = 0+) = N\cdot\delta(x - L/2) \tag{8}$$

With these boundary conditions,

$$A_n = \frac{2N}{L}\sin\left(\frac{n\pi}{L}\cdot\frac{L}{2}\right) = \frac{2N}{L}\sin\left(\frac{n\pi}{2}\right) \tag{9}$$

Hence, $A_{2m} = 0$, $A_{2m+1} = [2N/L](-1)^m$ and

$$p(x,t) = \frac{2N}{L}\sum_{m=0}^{\infty}(-1)^m \sin\left(\frac{(2m+1)\pi x}{L}\right)\exp\left[-\left(\frac{1}{\tau_p} + D_p\left(\frac{(2m+1)\pi}{L}\right)^2\right)t\right] \tag{10}$$

where N is the number of holes generated per unit area by exciton dissociation at the p/n interface. An identical equation, with appropriate substitution for the relaxation time and diffusion constant, describes the spatial/temporal behavior of the electrons. The simulated diffusion of the carriers with time under zero electric field is shown in Figure 6S under the assumption that the mobilities of the holes and electrons are equal: $\mu_n = \mu_p = 10^{-4}$ cm^2/V·s.

Electric Field Influence. If a built-in electric field is present or an external bias is applied, solutions for carrier distribution are in the form of eq 10, but with x replaced by $[x - \mu_p(F + F_{bi})t]$.[14] The built-in electric field is equal to the built-in potential, V_{bi}, divided by the thickness of the device, L. V_{bi} is equal to the difference in work functions, $\Delta\varphi$, of the front and back electrodes, or $F_{bi} = V_{bi}/L \approx \Delta\varphi/L = 0.5$ V/200 nm $= 2.5 \times 10^4$ V/cm. V_{bi} is a few tenths of a volt greater than the open circuit potential, V_{oc}, under the usual operating conditions.[12b] The built-in field acts to sweep the carriers away from the interface region and enhances or diminishes the applied electric field at reverse or forward bias, respectively.

Schematic diagrams of the energy levels in a bilayer photodiode under various conditions are shown in Figure 7S (Supporting Information). In the dark and with the electrodes interconnected by a conductor, the quasi-Fermi levels of both organic materials, as well as those of the two electrodes, are equalized, Figure 7S-a, and $V_{oc} = 0.0$. Photoexcitation creates excitons that dissociate to create free carriers in the p/n junction region, with the P3BT positive due to accumulation of photogenerated holes, and PV negative due to the accumulation of photogenerated electrons.

This charge separation causes an offset of the Fermi levels of the two organic layers and generates an open circuit voltage under illumination as shown in Figure 7S-b.[2b,12b] Application of a reverse bias enhances the internal electric field as shown in Figure 7S-c and facilitates the separation and migration of carriers toward the electrodes. When a forward bias is applied, the quasi-Fermi levels move in the opposite direction compared to reverse bias, and the diminished electric field ($F = F_{bi} - F_a$) in the device reduces the drift velocity and increases the probability of bimolecular recombination between electrons and holes. When the magnitude of the forward applied bias becomes greater than V_{bi}, then holes and electrons must tunnel through the p/n junction and travel in the direction opposite to that under short circuit, thus reversing the sign of the photocurrent, Figure 7S-d.

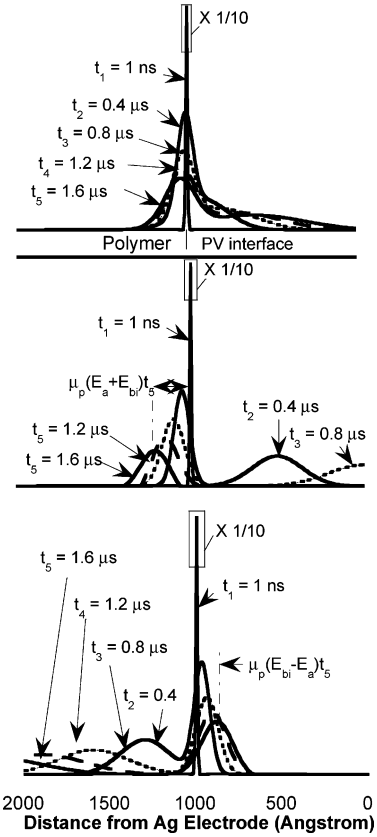

Figure 5. Simulated carrier concentration profiles undergoing diffusion and drift in an ITO/polymer/PV/Ag bilayer photocell. A thin sheet of carriers at $x = 1000$, produced by the light pulse, diffuse and drift under the influence of the applied and built-in electric fields: top to bottom, (a) short circuit; (b) applied reverse bias $= 10^5$ V/cm; (c) applied forward bias $= 10^5$ V/cm. The values, $\mu_p = 10^{-5}$ cm^2/V·s, $\mu_n = 10^{-4}$ cm^2/V·s, $F_{bi} = 2.5 \times 10^4$ V/cm, and $\tau_p = \tau_n = 0.1$ ms are assumed.

The distributions of carriers as calculated by eq 10 under the influence of the built-in electric field and the applied bias are shown in Figure 5. A thin carrier layer (holes in polymer side and electrons in PV side) is produced at the interface by the illumination pulse. The "hole packet" drifts toward the ITO electrode, and the "electron packet" drifts toward the Ag electrode under the influence of the built-in field as shown in Figure 5a. The drift velocity of each packet is directly proportional to the mobility of the carrier and to the total electric field, $v_d = \mu(F_a + F_{bi})$. In the simulations shown in Figure 5, the assumed electron mobility is greater than the hole mobility by a factor of 10, $\mu_n = 10^{-4}$ cm^2/V·s and $\mu_p = 10^{-5}$ cm^2/V·s. Application of a reverse bias enhances the drift caused by the built-in field as shown in Figure 5b. When a sufficiently large forward bias is applied (e.g., $V_{bi} - V_a < 0$), the photogenerated electrons in the PV must tunnel into the polymer and migrate toward the ITO electrode while holes must travel through the n-type material as shown in Figure 5c. The change of the carrier migration direction under forward

(14) Sze, S. M. *Physics of Semiconductor Devices*, 2nd ed.; John Wiley & Sons: New York, 1981.

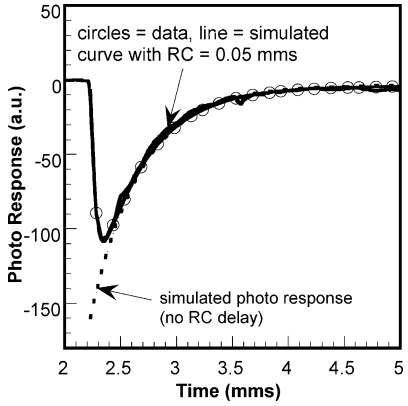

Figure 6. Simulated transient photoresponse following a 10-ns pulse of illumination: with no RC delay (dashed line). Solid line: dashed line multiplied by RC delay function and overlain on an experimental curve (simulation values: $\mu_p = \mu_n = 10^{-6}$ cm^2/V·s and $\tau_p = \tau_n = 4.5 \times 10^{-7}$ s; experimental conditions: $\lambda = 572$ nm, $F_a = -5 \times 10^4$ V/cm, $F_{bi} = 2.5 \times 10^4$ V/cm, $T = 298$).

bias is signaled by the change of sign of the transient photo voltage/current as observed in Figure 1, top. The effect of carrier lifetime on the simulated carrier concentration profile is shown in Figure 8S (Supporting Information), where an assumed shorter lifetime for the holes results in a more rapid decay of their initial concentration.

Influence of Carrier Lifetime and Mobility on the Transient Current Pulse. The transient current generated by carrier diffusion and drift in the bulk material after illumination pulse can be calculated (eq 1) by substituting the expressions for the carrier concentrations (eq 10) into eqs 4 and 5 to obtain

$$j(t) = \frac{q(F + F_{bi})}{L}\int_0^L (\mu_p p + \mu_n n)\, dx + \frac{q}{L}\int_0^L \left(D_n \frac{dn}{dx} - D_p \frac{dp}{dx}\right) dx \quad (11)$$

Equation 11 was solved numerically by integrating the electron and hole currents over the thickness of the organic layers ($L_1 + L_2$) (see Supporting Information for a description of the BASIC program). The simulated current vs time curves show that a very fast current spike is produced by the short pulse of light (Figure 6), corresponding to the essentially instantaneous formation of the very thin layer of carriers generated at the organic p/n interface. However, the RC time constant of the experimental circuit does not permit the determination of the nanosecond rise time of the initial production of carriers. However, the relatively slowly varying decay portion of the transient is little affected by the instrument response time. The solid curve in Figure 6 represents a convolution of the dashed curve with the instrument response function. The calculated curve is overlain on a plot of the experimental data to show the excellent agreement in the fit to the experimental curve.

Figure 7 shows the simulated transient photoresponse as a function of the applied electric field. A negative photocurrent is obtained at zero bias, and the peak height increases with increasing reverse bias. Application of a forward bias decreases the peak height until the photocurrent passes through zero and becomes

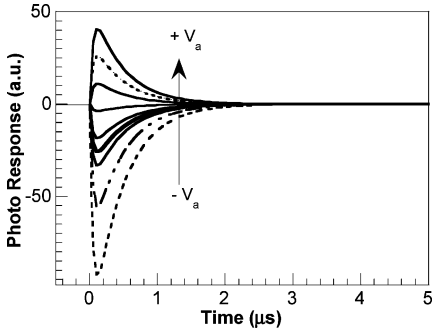

Figure 7. Simulated transient photoresponse as a function of different applied electric fields $\mu_p = \mu_n = 10^{-6}$ cm^2/V·s and $\tau_p = \tau_n = 4.5 \times 10^{-7}$ s.

positive when the applied bias exceeds the built-in electric field. A plot of the calculated peak photoresponse vs applied bias gives a linear relationship (Figure 9S (Supporting Information) in agreement with the experimental results shown in Figure 1.

The decay of the signal after the peak photoresponse results from two processes according to eqs 2 and 3: diffusive flow of free carriers in the bulk materials and first-order carrier trapping characterized by the trapping time τ_T ($=\tau_p$ or τ_n). Contributions to the space averaged current arise only from carriers that have escaped the e−h pair coulomb field, which in low-mobility semiconductors constitute a relatively low fraction. At such low carrier densities, bimolecular recombination between mobile carriers is not expected to be significant. Therefore, bimolecular recombination of carriers at the interface, which would further diminish the current signal with time, was ignored in this treatment. Although bimolecular recombination is not the primary cause of carrier loss, it is probably present and is most likely responsible for the sublinear response of the peak photocurrent to the light intensity (Figure 3) since a purely bimolecular decay gives a steady-state $j \propto \sqrt{I}$ dependence. Bimolecular recombination may also affect the rise time and peak amplitude of the photoresponse because the highest density of carriers occupies the region of the p/n junction immediately after the laser pulse.

The simulations reveal that the decay rate of the photoresponse curve is governed almost solely by the carrier lifetime, as shown by the normalized curves in Figure 8. For a given initial concentration of carriers, the peak height, j_p, is only weakly decreased as the carrier lifetime decreases (inset to Figure 8a). The dependence of the peak current on carrier lifetime arises because some carriers decay during the instrument response lag time in the rising portion of the curve. In contrast, changes in the mobilities of the carriers has very little effect on the decay rate, as shown by the normalized curves in Figure 8b; but the peak height, j_p, is strongly affected by the carrier mobility (inset to Figure 8b). These results agree with the qualitative reasoning presented earlier and with previous work in which it was concluded that the peak current depends only on the carrier mobility and the total charge generated during the light pulse, whereas the current in the decay portion of the curve is determined solely by the fraction of carriers that survive deep trapping.[15]

Therefore, the temperature dependence of the peak photocurrent may be ascribed to either or both of two

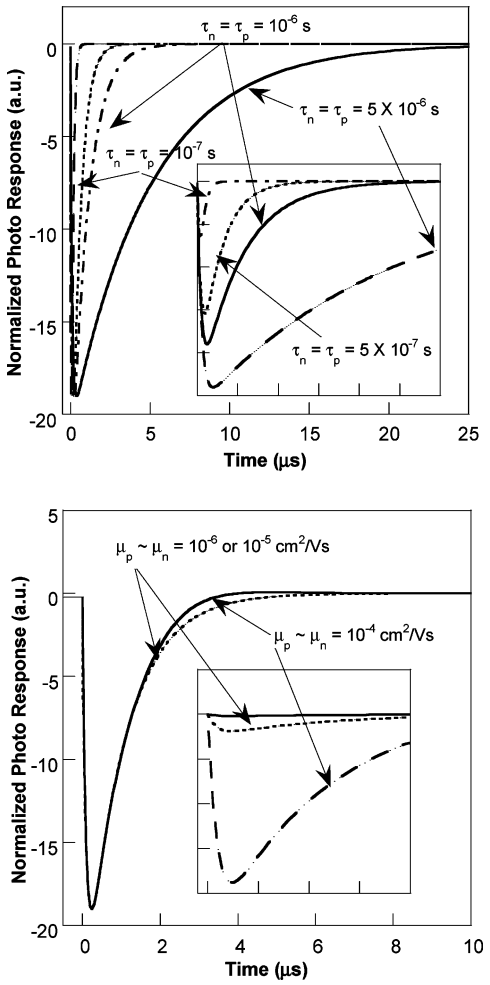

Figure 8. Simulated normalized transient photoresponse (insert: not-normalized) under short circuit: (top) $\mu_p = \mu_n = 10^{-6}$ cm^2/V·s; (bottom) $\tau_p = \tau_n = 10^{-6}$ s.

sources: the direct effect of temperature on exciton dissociation, that is, on the temperature dependence of the number of carriers $N_0(T)$, and/or the temperature dependence of the mobility. The Onsager model[16] has been employed successfully to treat the photogeneration of carriers in a variety of molecular solids. Using Onsager theory, Hughes[17] obtained the following expression for the yield of charge carriers from exciton dissociation,

$$N_0(T) = \phi_0(1 + eFr_0\epsilon_B/2k^2T^2)(\exp(-\epsilon_B/kT)) \quad (12)$$

where r_0 is the initial e−h separation, ϕ_0 is the quantum efficiency for geminate e−h pair production, and ϵ_B is the binding energy of the e−h pair. The temperature dependence of the carrier yield was not explicitly included in the present simulations; but, if the temperature dependence of j_p arises from thermally assisted charge carrier production, then the measured activation energies of 45−128 meV (field dependent) represent the activation energies for the carrier yield. These activation energies are far too low to be associated with carrier binding energy, ϵ_B, which is typically around 0.4 eV in conjugated molecular materials.[2c]

Therefore, the temperature dependence of j_p must arise from the temperature dependence of the carrier mobility. If the transport mechanism is carrier hopping due to thermal release of carriers from shallow traps, the effective mobility is given by the Hoesterey-Letson equation,[18]

$$\mu_{\text{eff}} = \frac{\mu_0}{1 + \rho_T \exp(\Delta\epsilon_T/kT)} \quad (13)$$

where ρ_T is approximately equal to the fraction of states available to carriers that are trap states and $\Delta\epsilon_T$ is the trap depth. When the second term in the denominator of eq 13 is large compared to unity, plots of $\ln(\mu_{\text{eff}})$ vs $1/T$ are linear and the trap depth may be obtained from the slope as shown in Figures 4 and 4S.

The Arhennius plots give relatively small activation energies, 40−150 meV, that are weakly field-dependent, decreasing with increasing field. Such weak field and temperature dependence can arise from highly ordered materials,[19] when there is both positional and energetic disorder present,[20] or when transport is controlled by grain boundaries[21] or by small polaron hopping.[22] Although our experimental range of temperatures is not great enough to distinguish between these models, a plot of $\ln(i_pT^{1.5})$ vs $1/T$ also gives good straight lines, from which a value for the polaron binding energy of ca. 200 meV can be extracted. This value is lower than the 800 meV measured for PPV[23] or the 1.2 eV measured for an aromatic amine-doped polystyrene.[24] Small activation energies for carrier mobilities, or even temperature-independent mobilities, have been observed many times for organic materials.[25]

If the mobility depends exponentially on the temperature, then one might expect that the decay rate ($1/\tau_T$) would also exhibit a strong temperature dependence via the relationship shown in eq 14,

$$1/\tau_T = N_T\sigma\nu \quad (14)$$

where N_T is the trap concentration, σ is the trap cross section, and ν is the carrier velocity and contains contributions from both the drift velocity and the thermal diffusion velocity, $\nu_{\text{therm}} \propto \sqrt{T}$. The observed weak temperature dependence of τ_T suggests that the carrier drift velocity is small compared to the thermal

(15) Donovan, K.; Movaghar, B.; Kreouzis, T. *Phys. Rev. B* **1998**, *58*, 3063.
(16) Onsager, L. *Phys. Rev.* **1938**, *54*, 554.
(17) Hughes, R. C. *Chem. Phys. Lett.* **1971**, *8*, 403 and 5442.
(18) Hoesterey, D. M.; Letson, G. M. *J. Phys. Chem. Solids* **1963**, *24*, 1609.
(19) Martin, S. J.; Kambali, A.; Walker, A. B. *Phys. Rev. B* **2003**, *67*, 165214.
(20) (a) Sin, J. M.; Soos, Z. G. *Philos. Mag.* **2003**, *83*, 901. (b) Martens, H. C. F.; Blom, P. W. M.; Schoo, H. F. M. *Phys. Rev. B* **2000**, *61*, 7489.
(21) (a) Horowitz, G.; Hajlaoui, M. E. *Synth. Met.* **2001**, *121*, 1349. (b) Horowitz, G.; Hajlaoui, M. E.; Hajlaoui, R. *J. App. Phys.* **2000**, *87*, 4456.
(22) Kreouzis, T.; Donovan, K. J.; Boden, N.; Bushby, R. J.; Lozman, O. R.; Liu, Q. *J. Chem. Phys.* **2003**, *118*, 8905.
(23) Osterbacka, R.; Wohlgenannt, M.; Shkunov, M.; Chinn, D.; Vardeny, Z. V. *J. Chem. Phys.* **2001**, *114*, 1797.
(24) Borsenberger, P. M.; Schein, L. B. *J. Phys. Chem.* **1994**, *98*, 233.
(25) (a) Shirota, Y. *J. Mater. Chem.* **2000**, *10*, 1. (b) Chesterfield, R. J.; Newman, C. R.; Pappenfus, T. M.; Ewbank, P. C.; Haukaas, M. H.; Mann, K. R.; Miller, L. L.; Frisbie, C. D. *Adv. Mater.* **2003**, *15*, 1278. (c) Genevičius, K.; Österbacka, R.; Juška, G.; Arlauskas, K.; Stubb, H. *Thin Solid Films* **2002**, *403*−*404*, 415. (d) Pandey, S. S.; Takashima, W.; Endo, T.; Rikukawa, M.; Kaneto, K. *Synth. Met.* **2001**, *121*, 1561. (e) Warman, J. M.; Gelinck, G. H.; de haas, M. P. *J. Phys. Condens. Matter* **2002**, *14*, 9935.

velocity (i.e., the mobility is low) and that the activation energy for deep trapping is very small.

The most effective traps, those with the largest cross sections, are localized charges of opposite sign to the carrier. These are coulomb-attractive traps and the carrier lifetime is determined primarily by the relatively high concentration of such traps near the p/n interface. The combination of structural disorder in packing and molecular configuration, chemical impurities, and interdiffusion of the p- and n-type layers is likely to create conditions for charged traps. In the presence of deep traps, the relaxation time is determined by the trapping time (τ_T), which is only weakly field- and temperature-dependent, chiefly through the field and temperature dependence of the carrier velocity. The observation of unpaired electrons by ESR in all the materials, even after extensive purification, is evidence that the organic materials contain potential traps produced during synthesis and handling by catalysts and/or environmental oxygen.[2,26] The photocurrent is predicted to relax exponentially with a temperature-independent rate constant of $1/\tau_T$ according to

$$j(t) \propto \exp(-t/\tau_T)$$

The transient decay tails of the normalized curves overlap each other, indicating the independence of carrier trapping on the electric field, at least in the limited range that was examined. The observed, small change of the decay rate between biased and unbiased measurements may arise from a difference in the concentration of unfilled traps due to the dark current that is present when a bias voltage is applied.

Conclusions

The kinetics of charge carrier decay and charge transport in an organic bilayer photocell were investigated using a transient excitation technique and model simulations. The peak photocurrent response is both field- and temperature-dependent, whereas the decay of the photoresponse, related directly to the carrier lifetime, was nearly independent of both temperature and field strength. The peak photocurrent is related to the light intensity by the expression $|j_p| = aI^k$, and the exponent, $k \approx 0.85$, is only weakly field-dependent. The temperature dependence of the peak photocurrent gives an activation energy that is significantly smaller than expected for the binding energy of a Frenkel exciton in a molecular solid and indicates that dissociation occurs predominately at sites associated with the organic p/n interface, and the exciton dissociation is neither thermally activated nor field-assisted. The low activation energy is therefore associated with the mobility. Weak temperature dependence of mobility in organic materials has been observed in many instances. In the range of fields tested, the mobility was also independent of the applied field.

For the P3BT-*co*-EDOT/PV cell employed in these experiments, the carrier lifetime is ca. 4.5×10^{-7} s. The apparent activation energy for carrier hopping ranged from 45 to 128 meV, increasing with decreasing electric field.

Acknowledgment. The authors gratefully acknowledge the financial support from NSF (Grant No. DMR-9986123) and Research Corporation (Grant No. N004285). Efficient programming by Dr. Steve Parus is gratefully acknowledged.

Supporting Information Available: Additional figures and details (PDF). This material is available free of charge via the Internet at http://pubs.acs.org.

CM035102D

(26) Abdou, M. S. A.; Lu, X.; Xie, Z. W.; Orfino, F.; Deen, M. J.; Holdcroft, S. *Chem. Mater.* **1995**, *7*, 631.